# Arousal regulates frequency tuning in primary auditory cortex

Pei-Ann Lin[a,1], Samuel K. Asinof[a,1], Nicholas J. Edwards[a], and Jeffry S. Isaacson[a,2]

[a]Center for Neural Circuits and Behavior, Department of Neurosciences, University of California San Diego, La Jolla, CA 92093

Edited by Eric I. Knudsen, Stanford University School of Medicine, Stanford, CA, and approved October 30, 2019 (received for review July 2, 2019)

**Changes in arousal influence cortical sensory representations, but the synaptic mechanisms underlying arousal-dependent modulation of cortical processing are unclear. Here, we use 2-photon $Ca^{2+}$ imaging in the auditory cortex of awake mice to show that heightened arousal, as indexed by pupil diameter, broadens frequency-tuned activity of layer 2/3 (L2/3) pyramidal cells. Sensory representations are less sparse, and the tuning of nearby cells more similar when arousal increases. Despite the reduction in selectivity, frequency discrimination by cell ensembles improves due to a decrease in shared trial-to-trial variability. In vivo whole-cell recordings reveal that mechanisms contributing to the effects of arousal on sensory representations include state-dependent modulation of membrane potential dynamics, spontaneous firing, and tone-evoked synaptic potentials. Surprisingly, changes in short-latency tone-evoked excitatory input cannot explain the effects of arousal on the broadness of frequency-tuned output. However, we show that arousal strongly modulates a slow tone-evoked suppression of recurrent excitation underlying lateral inhibition [H. K. Kato, S. K. Asinof, J. S. Isaacson, *Neuron*, 95, 412–423, (2017)]. This arousal-dependent "network suppression" gates the duration of tone-evoked responses and regulates the broadness of frequency tuning. Thus, arousal can shape tuning via modulation of indirect changes in recurrent network activity.**

brain state | inhibition stabilized network | lateral inhibition | signal correlation | noise correlation

Information processing in the sensory cortex is modulated by changes in behavioral states such as those associated with arousal, attention, or task engagement (1–4). Indeed, moment-to-moment changes in arousal have strong effects on spontaneous and stimulus-evoked firing activity in the primary visual (V1) (5–12) and auditory (A1) cortex (13–15). Despite the potential for arousal to regulate cortical sensory coding, the subthreshold synaptic mechanisms by which changes in brain state influence sensory representations and tuning properties are not well understood.

In recordings from head-fixed mice, changes in arousal are typically assessed by measurements of pupil diameter or exploratory behavior, such as locomotion, with increases in pupil diameter and bouts of running/walking indicating heightened arousal (1). Interestingly, the transition from quiet wakefulness to locomotion has different effects in the visual and auditory cortices: walking/running increases stimulus-driven firing in V1 (5, 6, 8, 10, 16) while it is associated with a decrease in sensory-evoked firing in A1 (13–15). However, heightened arousal does not require movement, and recent work suggests that motor feedback signals to the sensory cortex modulate activity differently than arousal tracked by pupillometry during quiet wakefulness (5, 13).

In this study, we use pupillometry and $Ca^{2+}$ imaging to study how fluctuations in arousal in the absence of locomotion modulate frequency coding in A1 of head-fixed mice. We show that, despite a reduction in frequency selectivity, elevated arousal improves frequency discrimination by L2/3 pyramidal cells. In vivo whole-cell current- and voltage-clamp recordings from L2/3 cells reveal how changes in membrane potential dynamics and tone-evoked synaptic input contribute to this arousal-dependent modulation of frequency representations.

## Results

We used transgenic mice expressing the $Ca^{2+}$ indicator GCaMP6s [Emx-Cre;CamKII-tTA;Ai94(TITL-GCaMP6s)] (17) and 2-photon imaging (950 nm) to study tone responses in A1 L2/3 pyramidal cells ($n = 8$ imaging fields, 5 mice). Prior to recording, head-fixed mice were habituated to sitting quietly for prolonged time periods (1 to 2 h) on a static platform. During imaging of A1 in the right hemisphere, mice sat on a passive treadmill that measured movement while an IR camera simultaneously monitored the pupil (illuminated by IR laser emission through the eye) of the contralateral eye and blocks of pure tones (17 log spaced frequencies, 2–40 kHz, 1 s duration, 3 s ITI, 60 dB) were delivered to the contralateral ear (Fig. 1*A*). During single imaging sessions, pupil diameter (normalized to maximum pupil diameter) fluctuated between constricted and dilated states (Fig. 1*B*). Under our conditions, mice were predominantly stationary, and while sporadic locomotion bouts were associated with maximally dilated pupils, mice spent considerable time with pupils just as dilated while stationary (Fig. 1 *B* and *C*). For all experiments ($n = 8$), we excluded the small number of trials during locomotion and, thus, limited our investigation to how arousal (indexed by pupil diameter) modulated cortical activity.

We examined the influence of arousal by sorting tone trials by the mean pupil diameter during the tone. While responses were rarely observed when pupils were most constricted (1–20% of maximal diameter), the same tones elicited robust responses as pupil diameter increased (Fig. 1*D*). This reflects the fact that both the amplitude and the reliability of tone-evoked responses were strongly dependent on arousal. At best frequency ([BF], the frequency eliciting the strongest response in each cell averaged across all pupil diameters unless stated otherwise), the response amplitude and trial-to-trial reliability increased more than 4-fold (Friedman's ANOVA, $P < 0.001$) when pupils were most dilated [81–100% vs. 1–20% maximal diameter (Fig. 1$E_1$)]. These

### Significance

**Changes in brain state modulate how information is processed in sensory cortical areas. Here we use population imaging and intracellular recording to show that arousal regulates frequency tuning in layer 2/3 of primary auditory cortex. Increased arousal reduces lateral inhibition, broadens frequency tuning and enhances cortical representations of pure tones. Despite the arousal-dependent reduction in stimulus selectivity, frequency discrimination by cell ensembles improves due to a reduction in correlated variability (noise correlations).**

Author contributions: P.-A.L., S.K.A., N.J.E., and J.S.I. designed research; P.-A.L., S.K.A., and N.J.E. performed research; P.-A.L., S.K.A., N.J.E., and J.S.I. analyzed data; and P.-A.L., S.K.A., and J.S.I. wrote the paper.

The authors declare no competing interest.

This article is a PNAS Direct Submission.



[1]P.-A.L. and S.K.A. contributed equally to this work.

[2]To whom correspondence may be addressed. Email: jisaacson@ucsd.edu.

First published November 22, 2019.

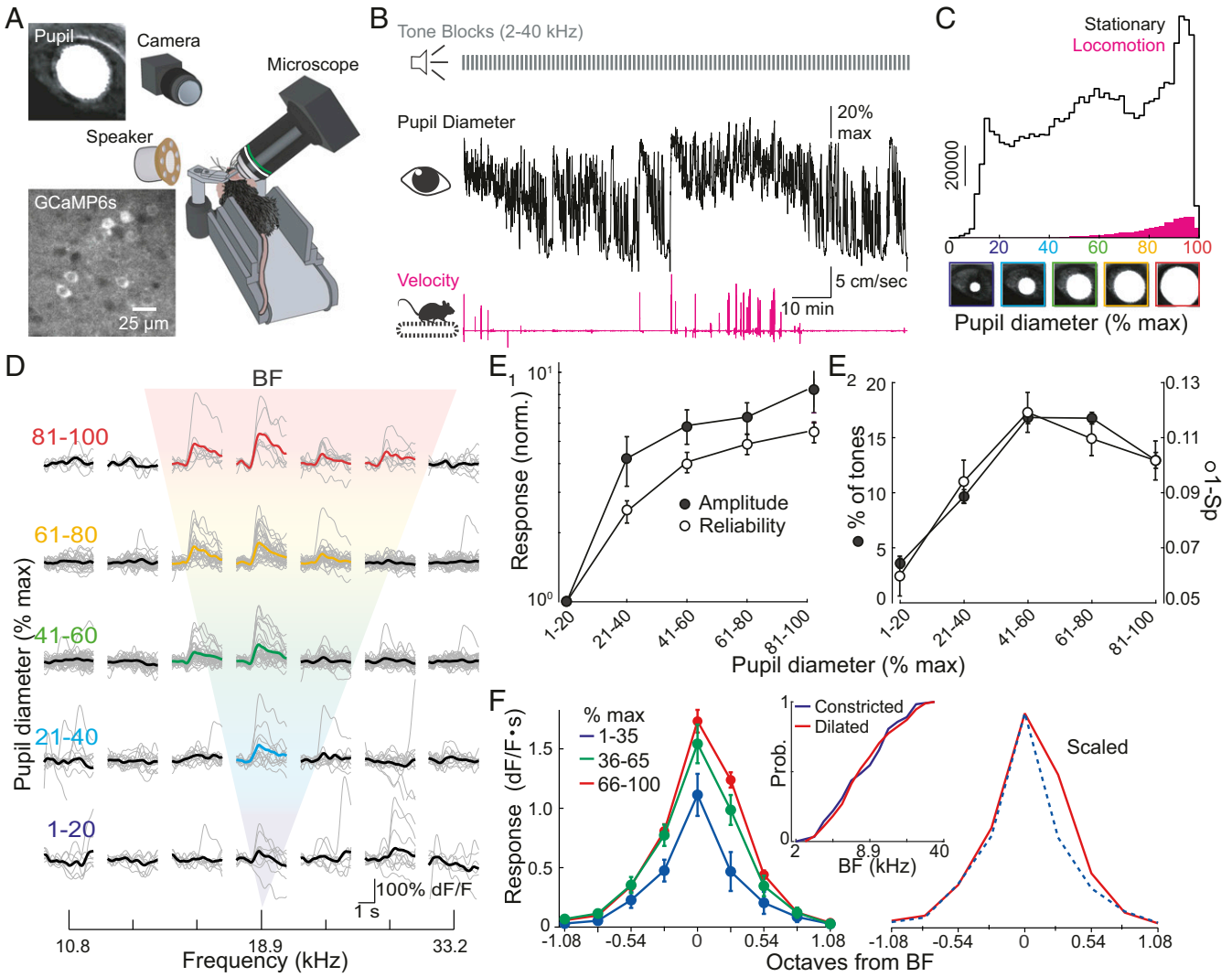


**Fig. 1.** Arousal modulates frequency tuning of L2/3 pyramidal cells. (*A*) Experiment schematic. An IR camera records pupil size (*Top Left*) during imaging of GCaMP6s-expressing neurons (*Bottom Left*). (*B*, *Top*) Tones presented during imaging. (*B*, *Middle*) Pupil diameter for 1 experiment. (*B*, *Bottom*) Simultaneous recording of mouse velocity. (*C*) Summary of pupil diameters ($n = 8$ experiments) when mice were stationary (black) or walking (pink) shows that locomotion only occurred during high arousal and mice were typically stationary. (*D*) A representative cell showing enhancement of tone-evoked responses as arousal (pupil diameter) increases. Bold trace, average response. Colored bold traces indicate frequencies eliciting a significant response. Gray, individual trial. ($E_1$) Arousal increases the amplitude (filled circles) and reliability (open circles) of BF responses ($n = 195$ cells). ($E_2$) Arousal increases percentages of tones evoking significant responses (filled circles) and reduces lifetime sparseness (Sp) (1-Sp, open circles). (*F*) Arousal broadens frequency tuning curves. (*Left*) Average tuning ($n = 195$ cells) during low (blue), moderate (green), and high (red) arousal aligned to low arousal BF. (*Right*) Low and high arousal curves scaled. (*Middle*) Cumulative probability plots show no shift in BF (1–35% [Constricted] vs. 66–100% [Dilated] maximum diameter, $n = 119{,}186$ cells). Error bars, SEM.

changes in response strength led to a marked increase (Friedman's ANOVA, $P < 0.001$) in the broadness of frequency tuning of individual cells: The number of tones eliciting significant responses peaked at moderate arousal levels (41–60% of maximal pupil diameter, Fig. 1$E_2$). Similar results were obtained using lifetime sparseness (18) (Friedman's ANOVA, $P < 0.001$), a tuning measure that does not require thresholding (Fig. 1$E_2$). We examined whether arousal modulates the shape of frequency tuning curves by centering cell responses to their BF at low arousal (Fig. 1*F*). Intriguingly, increases in arousal widened frequency tuning curves ($n = 119$ cells; 2-way ANOVA, $P_{\text{arousal}}$, $P_{\text{frequency}}$, and $P_{\text{arousal-frequency interaction}} < 0.001$) in an asymmetric fashion: responses to frequencies >BF were more strongly enhanced than responses to frequencies <BF (low vs. high arousal post hoc comparisons, $P = 0.06$ and <0.001 for −0.27 octaves and +0.27 octaves from BF, respectively). Despite arousal-dependent changes in the symmetry of tuning curves, the BF of individual cells remained constant (Kolmogorov–Smirnov test, $P = 0.94$, Fig. 1*F*). These results indicate that arousal strongly shapes the strength of tone-evoked responses and broadens frequency tuning in L2/3.

We next considered how arousal-dependent changes in pyramidal cell response properties contribute to sensory representations in A1. Consistent with the increases in response strength and tuning broadness, the fraction of cells responding to tones increased with arousal (Friedman's ANOVA, $P < 0.001$, Fig. 2 *A* and *B*). These results indicate that arousal shapes the relative sparseness of sensory representations at the population level.

How do arousal-related changes in sensory representations impact the ability of the pyramidal cell population to discriminate frequencies? At face value, the reduction in sparseness of activated cells and broadening of frequency tuning should increase overlap in cell ensembles activated by different frequencies. This implies that increased arousal would degrade rather than improve frequency discrimination. To address this, we analyzed interneuronal

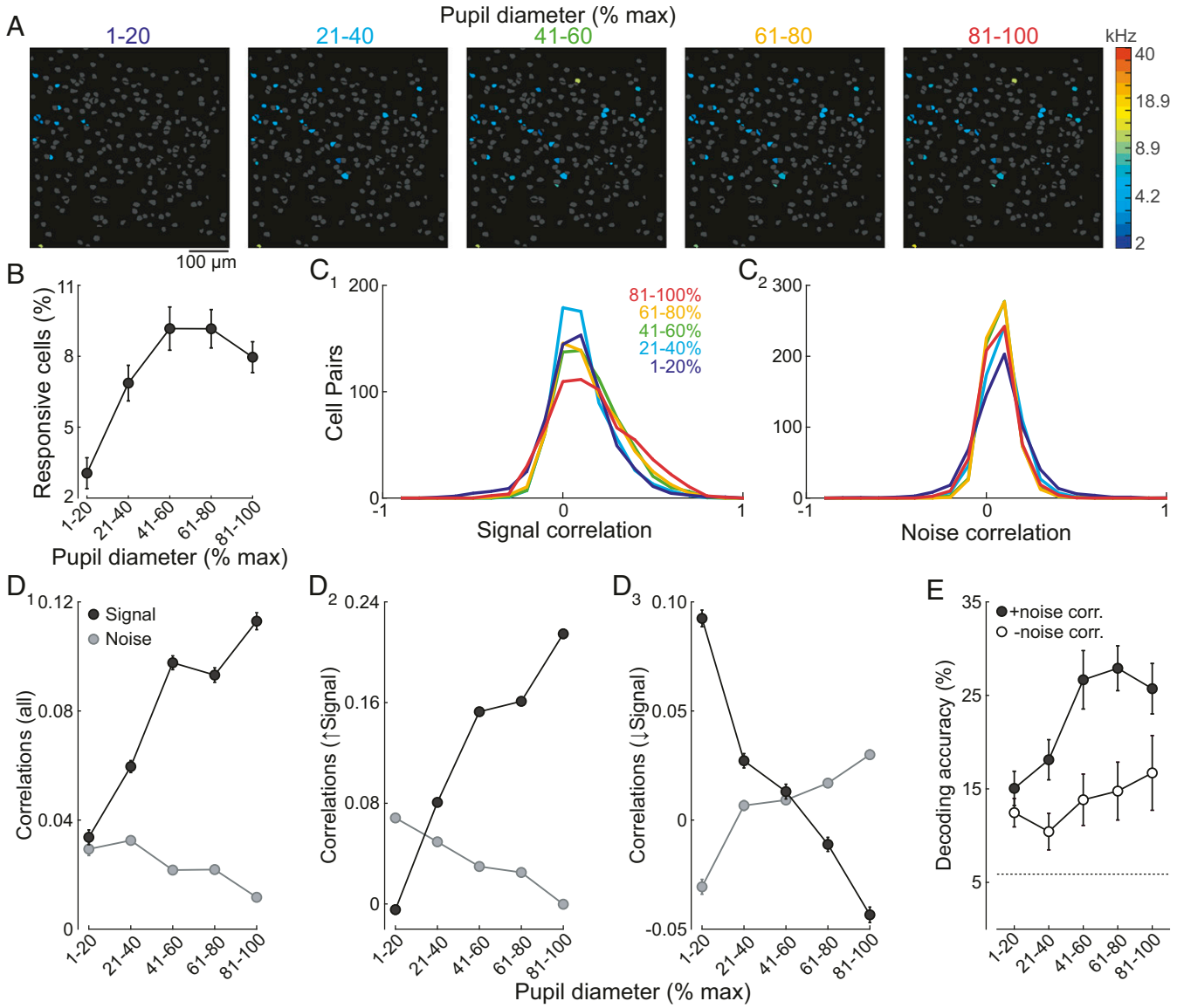


**Fig. 2.** Elevated arousal decreases sparseness of tone representations and improves frequency discrimination via modulation of noise correlations. (*A*) Increased arousal results in more tone-responsive cells. Responsive cells color coded by BF within the same field at different levels of arousal. Nonresponsive cells, gray. (*B*) Summary of tone responsiveness ($n$ = 8 fields). ($C_1$) Increased arousal results in broader $r_{signal}$ distributions and narrower $r_{noise}$ distributions ($C_2$, $n$ = 4,938 cell pairs). ($D_1$) Arousal differentially modulates $r_{signal}$ (black) and $r_{noise}$ (gray). ($D_2$) For the majority of cell pairs ($n$ = 3,086), arousal increases $r_{signal}$ and decreases $r_{noise}$. ($D_3$) The opposite relationship can also be observed ($n$ = 1,852). (*E*) Nonlinear classifier analysis reveals that arousal-dependent increases in decoding accuracy are due to changes in $r_{noise}$. Filled circles, $r_{noise}$ intact. Open circles, $r_{noise}$ removed. Error bars, SEM.

correlations that contribute to population coding: signal correlations ($r_{signal}$), a measure of tuning similarity between pairs of neurons and noise correlations ($r_{noise}$), a measure of how much the trial-to-trial response variability of a pair of neurons is correlated (19, 20). Consistent with previous studies in the auditory cortex (21–24), mean $r_{signal}$ and $r_{noise}$ values were small and positive ($n$ = 4,938 cell pairs, 8 experiments, Fig. 2 *C* and $D_1$). Interneuronal correlations were significantly modulated by arousal (Fig. 2*C*, 2-way ANOVA, $P_{arousal}$, $P_{correlations}$, and $P_{interaction}$ <0.001). Across all cells, $r_{signal}$ increased markedly as pupils became more dilated (Fig. 2$D_1$). This indicates that the tuning of pyramidal cells became more similar as arousal increased, consistent with the notion that elevations in arousal could degrade frequency discrimination. However, $r_{noise}$ fell as arousal increased (Fig. 2$D_1$). Previous work has established that reducing $r_{noise}$ should enhance sensory discrimination when cell pairs exhibit more similar tuning but impair discrimination when tuning becomes dissimilar (19, 20, 24–26). Intriguingly, we found that arousal-dependent changes in $r_{noise}$ were highly selective: $r_{noise}$ decreased specifically in cell pairs that became more similarly tuned (increase in $r_{signal}$) as arousal increased (2-way ANOVA, $P_{arousal}$, $P_{correlations}$, and $P_{interaction}$ < 0.001, Fig. 2$D_2$). In contrast, $r_{noise}$ increased specifically for cell pairs in which elevated arousal led to a reduction in $r_{signal}$ (2-way ANOVA, $P_{arousal}$, $P_{interaction}$ < 0.001, and $P_{correlations}$ = 0.066, Fig. 2$D_3$). Together, these relationships between $r_{signal}$ and $r_{noise}$ predict that increases in arousal should enhance frequency discrimination by L2/3 cell populations.

To investigate the net effect of arousal on frequency discrimination, we used a nonlinear classifier (K-nearest neighbors', *Materials and Methods*). To specifically investigate the contribution of arousal-dependent changes in noise correlations to frequency encoding, the temporal order of responses was shuffled such that noise correlations were abolished while the frequency

identity for each tone trial remained unchanged. As expected, the decoder performed above chance level (5.9%) independent of arousal for both the unshuffled and the shuffled datasets. More importantly, decoding accuracy improved significantly (Fig. 2*E*) only when the data were unshuffled (2-way ANOVA with post hoc multiple comparisons, $P_{\text{arousal}}$, $P_{\text{dataset}} < 0.001$, and $P_{\text{interaction}} = 0.127$). Thus, changes in noise correlations play an important role in improving frequency discrimination as arousal increases.

We next used whole-cell recording to measure how arousal impacts subthreshold activity in L2/3 cells. Studies in many cortical areas indicate that spontaneous membrane potential ($V_m$) dynamics are influenced by brain state (reviewed in ref. 1). Indeed, during low to moderate arousal, current-clamp recordings revealed large-amplitude low-frequency (2–10 Hz) $V_m$ fluctuations that were attenuated at high levels of arousal (Fig. 3 $A_1$ and $A_2$). Both $V_m$ SD and low-frequency oscillations (2–10 Hz power) diminished during high arousal ($n = 10$, Friedman's ANOVA, $P = 0.025$ and 0.020, respectively, Fig. 3$A_3$), consistent with previous studies tracking locomotion or pupil diameter in V1 and A1 (7, 8, 10, 11, 14). Similar to deep layer neurons in A1 (14), mean $V_m$ was slightly more hyperpolarized during moderate arousal ($n = 26$, Friedman's ANOVA, $P = 0.019$, Fig. 3$A_4$). Despite the similarity in mean $V_m$ during the lowest and highest levels of arousal, the rate of spontaneous spiking steadily declined as arousal increased ($n = 18$, 7 whole-cell and 11 cell-attached recordings, Friedman's ANOVA, $P = 0.005$, Fig. 3$A_4$). Together, these findings are consistent with the idea that low arousal is associated with high $V_m$ variability and slow synchronized cortical activity while high arousal enforces low variability, suppression of slow rhythms and fewer spontaneous spikes (1, 5, 7, 15).

In agreement with recent work characterizing lateral inhibition in A1 (27), tones (100–200 ms) at "preferred" frequencies evoked short-latency excitatory postsynaptic potentials (EPSPs) while distal ("nonpreferred") frequencies evoked a slow hyperpolarization (Fig. 3*B*). Interestingly, the time course of responses to preferred tones was arousal dependent. Averaging responses during low arousal revealed that the short-latency EPSP was curtailed by membrane hyperpolarization (Fig. 3*B*). During higher arousal, although the early amplitude of the EPSP slightly increased, the EPSP duration was markedly prolonged. For responses at nonpreferred frequencies, the tone-evoked hyperpolarization was strongly suppressed as arousal increased (Fig. 3*B*). Given the small change in the early EPSP, the most parsimonious explanation for the increased duration of preferred responses is the suppression of the overlapping slow hyperpolarization.

We quantified arousal-dependent changes in tone-evoked responses across cells by aligning responses to each cells' BF (Fig. 3$C_1$). On average, increases in arousal were associated with modest increases in EPSP peak amplitude ($n = 15$, 2-way ANOVA, $P_{\text{frequency}} < 0.001$, $P_{\text{arousal}} = 0.033$, and $P_{\text{interaction}} = 0.994$, Fig. 3$C_2$). However, arousal had a strong effect on the response integral and duration of tone-evoked EPSPs. During



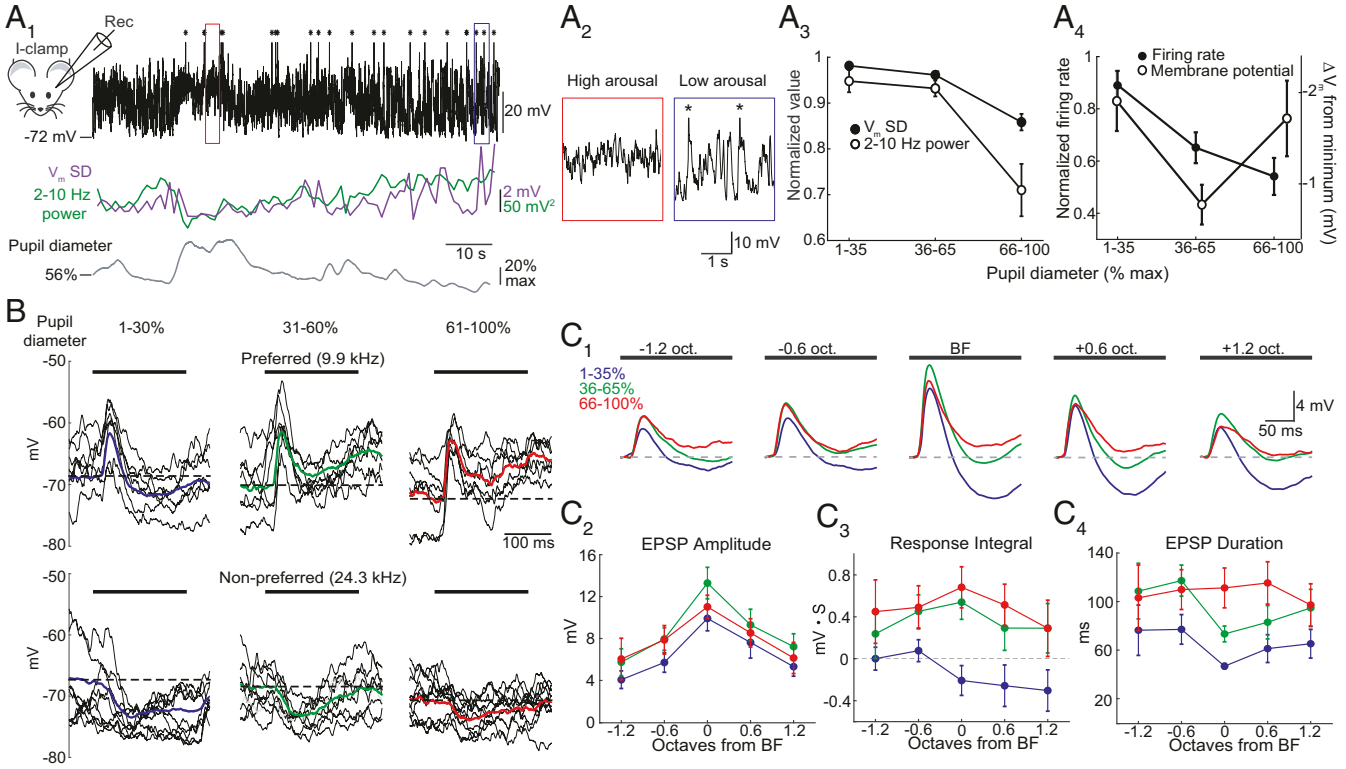


**Fig. 3.** Elevated arousal reduces membrane potential variability, spontaneous firing, and lateral inhibition. ($A_1$, *Top*) Current-clamp recording of membrane potential ($V_m$) in a representative L2/3 cell. Asterisks mark truncated action potentials. (*Middle*) $V_m$ SD (purple) and 2–10 Hz power (green) over 1 s intervals. (*Bottom*) Pupil diameter. ($A_2$) Expansion of areas marked in $A_1$. ($A_3$) Summary showing that as arousal increases, 2–10 Hz power (open circles) and SD (filled circles) decrease. ($A_4$) Summary showing that spontaneous firing decreases as arousal increases (filled circles, $n = 19$). Mean $V_m$ is most hyperpolarized during moderate arousal (open circles, $n = 30$ cells). (*B*) Responses to a preferred (*Top*) and nonpreferred (*Bottom*) tone (black bar) during different arousal levels in a representative cell. Gray, subset of single trials. Bold, mean response. Dashed line, baseline $V_m$. ($C_1$) Average responses to tones aligned to BF of each cell during low (blue), moderate (green), and high (red) arousals ($n = 15$ cells). Dashed line, baseline $V_m$. ($C_2$) Arousal causes a modest increase in EPSP peak amplitude. ($C_3$) Responses shift from net hyperpolarization to net depolarization for tones ≥BF. ($C_4$) Arousal-dependent suppression of lateral inhibition increases EPSP duration. Error bars, SEM.

low arousal, tone-evoked hyperpolarization was most prominent during BF tones (frequencies with the strongest early EPSP) and those of higher frequencies. As arousal increased, suppression of the slow hyperpolarization shifted the integrated responses from net hyperpolarization to net depolarization (2-way ANOVA, $P_{\text{frequency}} = 0.458$, $P_{\text{arousal}} < 0.001$, and $P_{\text{interaction}} = 0.943$, Fig. $3C_3$) and EPSP duration was prolonged (2-way ANOVA, $P_{\text{frequency}} = 0.303$, $P_{\text{arousal}} < 0.001$, and $P_{\text{interaction}} = 0.806$, Fig. $3C_4$). Interestingly, the differences in response integral and EPSP duration between low and high arousal states were largest for frequencies ≥BF (Fig. 3 $C_3$ and $C_4$). Together, these results indicate that arousal can regulate response strength by reducing a form of lateral inhibition that limits the duration of tone-evoked synaptic excitation.

What accounts for the arousal-dependent changes in tone-evoked synaptic potentials? To address this question, we used voltage clamp to isolate excitatory postsynaptic currents (EPSCs) in L2/3 cells ($V_{\text{hold}} = -70$ mV, near the reversal potential for inhibition set by our internal solution). Under resting conditions, cells received high-frequency barrages of spontaneous EPSCs (Fig. 4*A*). On individual trials, preferred tones evoked transient EPSCs locked to tone onset (ON response). During low arousal, transient ON responses were immediately followed by a sustained suppression of spontaneous EPSCs. When trials were averaged, this resulted in a slow outward current (relative to baseline). We have recently shown (27) that this reflects a reduction in ongoing recurrent activity, "network suppression (NS)," underlying an unconventional form of lateral inhibition that shapes frequency tuning. Indeed, during low arousal, NS was strongest at nonpreferred frequencies (Fig. 4 *A* and $E_1$). Thus, the slow tone-evoked hyperpolarization in current-clamp recordings is due to a suppression of recurrent excitation rather than direct synaptic inhibition (27). Intriguingly, while early ON responses were only slightly modulated, NS was strongly attenuated when arousal increased (Fig. 4 *A* and *C*–*E*). This loss of NS led to an increase in duration of ON responses (Fig. 4*A*). These results suggest that NS limits the strength of tone-evoked excitation in an arousal-dependent manner.

One explanation for the arousal-dependent attenuation of NS is that elevated arousal itself suppresses spontaneous excitation. In other words, during high arousal, there might be less synaptic input to suppress. We, thus, examined the relationship between arousal and spontaneous activity. Consistent with membrane voltage recordings, barrages of large-amplitude EPSCs during low arousal became desynchronized when arousal increased (Fig. 4 $B_1$ and $B_2$). Although this led to a marked change in current variability (Friedman's ANOVA, $P < 0.001$), total current (mean $I_{\text{m}}$) remained constant (Friedman's ANOVA, $P = 0.223$, and $n =$ 14 cells, Fig. 4 $B_3$ and $B_4$). Thus, while excitatory input was more variable on a moment-to-moment basis during low arousal, the net amount of ongoing synaptic excitation remained the same as arousal increased. This indicates that arousal-dependent changes in NS cannot be due to changes in the available amount of recurrent excitation.

Given that inhibitory interneurons are highly interconnected with recurrent excitatory circuits, changes in NS should also

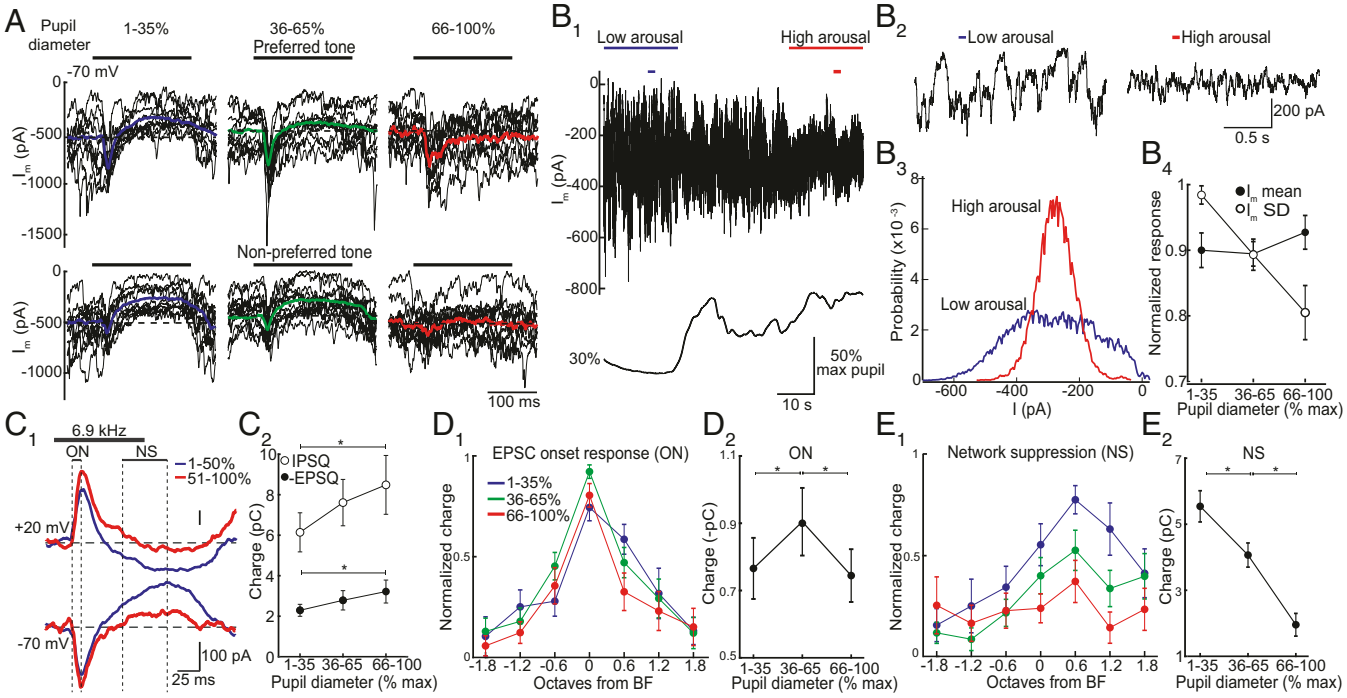


**Fig. 4.** Arousal modulates network suppression underlying lateral inhibition. (*A*) EPSCs in response to a preferred (*Top*) and nonpreferred (*Bottom*) tone during different arousal levels from 1 cell. Gray traces, subset of single trials. Bold traces, average. Dashed line, baseline. (*B*) Loss of network suppression is not due to less spontaneous excitation. ($B_1$) Current (−70 mV) and pupil diameter from 1 cell show a decrease in current variability during increased arousal. ($B_2$) Expansion of periods marked by small bars in $B_1$. ($B_3$) All points histogram of current (20 s) from $B_1$. ($B_4$) Increases in arousal decrease current variability ($I_{\text{m}}$ SD) while mean current is unchanged ($n = 14$ cells). (*C*) Arousal modulates EPSCs and IPSCs similarly. ($C_1$) Averaged tone-evoked EPSCs and IPSCs from the same cell during different arousal states. ($C_2$) Absolute charge above (below) baseline for IPSCs (EPSCs) during different arousal levels ($n = 35$ tone responses at each arousal level, 12 cells, $^*P = 0.010$ and 0.048, respectively, paired *t* test). (*D*) EPSC onset (ON) responses in $C_1$) peak during moderate arousal. ($D_1$) Normalized ON responses aligned to BF ($n = 16$ cells). ($D_2$) Summary of all significant ON responses recorded at each arousal level shows that ON component increased from low to moderate arousal and then decreased during high arousal ($^*P < 0.003$, paired *t* test, and $n = 32$ frequencies,16 cells). (*E*) NS of EPSCs (in $C_1$) was biased to high frequencies and decreased monotonically with increasing arousal. ($E_1$) Normalized NS aligned to BF ($n = 16$ cells). ($E_2$) Summary of significant responses shows that NS steadily decreased with increases in arousal ($^*P < 0.001$, paired *t* test, and $n = 27$ frequencies, 11 cells). Error bars, SEM.

impact tone-evoked synaptic inhibition (27). We, thus, compared the effect of arousal on tone-evoked EPSCs ($V_{hold}$ = −70 mV) and inhibitory postsynaptic currents (IPSCs, $V_{hold}$ = +20 mV, near the reversal potential for excitation) in the same cells ($n$ = 12). Tone-evoked NS of IPSCs mirrored suppression of EPSCs (Fig. 4$C_1$). Moreover, arousal-dependent changes in the strength of tone-evoked excitation and inhibition (total charge below and above baseline, respectively) scaled such that the relative balance of excitation/inhibition remained constant (1.38- and 1.40-fold changes from low to high arousal states for IPSCs and EPSCs, respectively, Fig. 4$C_2$).

We next considered how arousal modulated the tuning of tone-evoked excitation. Overall, short-latency ON responses were largest during moderate arousal ($n$ = 16 cells, Fig. 4 $D_1$ and $D_2$). However, changes in arousal did not have an obvious impact on ON response tuning (2-way ANOVA, $P_{frequency} < 0.001$, $P_{arousal} = 0.236$, and $P_{interaction} = 0.585$). In contrast, increases in arousal led to a stronger monotonic attenuation of tone-evoked network suppression (2-way ANOVA, $P_{frequency}$, $P_{arousal} < 0.002$, and $P_{interaction} = 0.539$, Fig. 4 $E_1$ and $E_2$). Furthermore, the arousal-dependent change in NS appeared tuned to frequencies ≥BF. This reflects the fact that NS itself is biased to high frequencies (27). Together, these results indicate that, while arousal weakly modulates short-latency excitation, it has a strong impact on tone-evoked responses via regulation of an indirect form of inhibition that gates recurrent excitation.

## Discussion

In this study, we used pupillometry, $Ca^{2+}$ imaging, and intracellular recording in stationary mice to investigate arousal-related changes in frequency-tuned activity in A1. Imaging activity evoked by pure tones in L2/3 pyramidal cells revealed that arousal-dependent increases in response amplitude and reliability decreased the sparseness of cortical tone representations. Consistent with these changes, signal correlations increased with arousal indicating greater overlap in the frequency-tuning curves of cells across the cortical population. Despite this increase in tuning similarity, elevated arousal improved frequency discrimination by cell ensembles due to a reduction in noise correlations (shared trial-to-trial variability). Similar to previous studies (1, 7, 11, 14), increases in arousal caused a shift in spontaneous synaptic activity: slow (2–10 Hz) bursts of excitatory input gave way to steady desynchronized input. Slow oscillations in spontaneous activity can be correlated between nearby cells as well as across wide areas of the sensory cortex (28). Therefore, we think it likely that the arousal-dependent shift in membrane dynamics is largely responsible for the reduction in noise correlations underlying improved frequency discrimination.

Increases in arousal were associated with a reduction in frequency of spontaneous action potentials, raising the possibility that the changes in sensory representations we observed simply reflect an enhanced signal-to-noise-ratio (SNR). Indeed, the arousal-dependent increase in response strength and reliability as well as the reduction in sparseness could be due to an improved SNR. However, increases in arousal also broadened frequency-tuning curves of individual cells due to a stronger enhancement of frequencies >BF. Thus, while changes in SNR are likely to contribute to modulation of cortical tone representations, SNR alone cannot explain the effects of arousal on frequency tuning.

We used current- and voltage-clamp recordings to examine how arousal-dependent changes in tone-evoked subthreshold activity could modulate tuning properties. Interestingly, conventional short-latency tone-evoked synaptic excitation was affected by arousal in a nonmonotonic fashion. Transitions from low to moderate arousals led to a modest increase in the strength of short-latency evoked EPSCs, however, response strength subsequently declined during high arousal. Activity evoked by complex sounds in deep layers of A1 is similarly found to be maximal during moderate arousal (14). Nonetheless, the small arousal-related increases in conventional short-latency synaptic input seem insufficient to account for the strong changes in activity observed with $Ca^{2+}$ imaging.

We show here and in recent work in awake mice (27) that nonpreferred tones can evoke a pure inhibitory response due to a slow suppression of ongoing recurrent synaptic excitation. This network suppression relies on cortical somatostatin-expressing interneurons and provides an unconventional form of lateral inhibition (27). Recent work in V1 indicates that surround suppression also reflects a reduction in total network input due to somatostatin interneurons (29). Here, we show that NS is strongest during low arousal and becomes progressively weaker as arousal increases. Furthermore, the arousal-dependent loss of NS at preferred frequencies leads to an increase in duration of tone-evoked responses. Intriguingly, NS occurs preferentially for tones >BF (27). Although the reasons for this asymmetry are yet to be established, the net effect of the strong reduction in NS by arousal is a preferential change in synaptic responses to high-frequency tones. This asymmetry in NS is likely to account for why increases in arousal broaden frequency tuned L2/3 cell output with a high-frequency bias.

## Materials and Methods

Mice [8–16 wk old, Emx1-Cre (Jackson Laboratories No. 05638), Ai94(TITL-GCaMPs)-D;CaMK2a-tTA (Jackson Laboratories No. 024115) or wild-type C57Bl6] were housed with a 12:12 h reversed light cycle. Experiments were performed during the dark period. All procedures were in accordance with protocols approved by the University of California San Diego Institutional Animal Care and Use Committee and guidelines of the National Institutes of Health.

**Surgical Preparation.** For imaging, mice were anesthetized with isoflurane and received dexamethasone (2 mg/kg, i.m.). A custom head bar was glued to the skull, muscle overlying the right auditory cortex was removed, and a craniotomy (~2 × 3 mm) was performed over the auditory cortex, leaving the dura intact. A glass window was placed over the craniotomy and secured with dental acrylic. Mice received baytril (10 mg/kg) and buprenorphine (0.1 mg/kg) before returning to their home cages. Mice were habituated to sitting quietly while head fixed for 2–7 d (2 h/day) before imaging.

For electrophysiology, 1–3 d after head-bar implantation and habituation to head fixation, mice were anesthetized with isoflurane, and the skull above A1 identified by intrinsic imaging (30) was thinned using a drill. During thinning, the skull was flushed with cold artificial cerebrospinal fluid ([aCSF], [in millimoles] 142 NaCl, 5 KCl, 10 glucose, 10 Hepes, 3.1 $CaCl_2$, 1.3 $MgCl_2$, pH 7.4, 310 mOsm). After thinning, mice received dexamethasone (2 mg/kg) and recovered in their home cage for >2 h. Immediately prior to recording, a well filled with aCSF was constructed around the recording site, a small (<0.3 mm) craniotomy was performed in the thinned skull, and the dura removed.

**Pupillometry and Locomotion Tracking.** The eye contralateral to imaging or recording was monitored via a camera (BFLY-U3-05S2M-CS, Point Gray). For electrophysiology experiments, an IR LED was used to visualize the pupil in the presence of weak ambient illumination (473 nm). Locomotion was monitored by a passive treadmill fitted with a rotary encoder (Janelia). Pupil measurements and velocity were acquired using open-source software (Bonsai, http://bonsai-rx.org/). Pupil diameter values were smoothed using a moving average filter (1 s). Locomotion epochs (nonzero velocity for >0.5 s) were excluded from analysis. Pure tones were delivered via a calibrated free-field speaker (ES1, TDT) directed to the ear contralateral to imaging or recording. Tones were generated by software (BControl; http://brodylab.org) running on MATLAB (MathWorks) communicating with a real-time system (RTLinux).

**In Vivo Two-Photon $Ca^{2+}$ Imaging.** Imaging was performed within 2 to 3 wk of window implantation. Imaging fields were within A1 determined from intrinsic signal imaging. GCaMP6s was excited at 950 nm (Mai Tai, Newport), and images (512 × 512 pixels covering ~500 × 500 μm) were acquired at 28.4 Hz with a 16× objective (Nikon) using a commercial microscope (B-scope, Thorlabs) and ScanImage4. Images were acquired 120–250 μm below the dura, and lateral motion was corrected using a phase correlation algorithm (https://github.com/cortex-lab/Suite2P).

**Imaging Analysis.** Responses were classified as significant if $P < 0.005$ (Wilcoxon rank sum test) for >85% of trial-pooled timepoints over any continuous 0.5 s window during the 1 s tone, compared to a trial-pooled 1 s period preceding the tone. Cells were responsive if responses to, at least, 2 tones in, at least, 2 of 5 arousal levels (bin size 20% from 0 to 100% pupil max) were significant. Response strength was measured as the *dF/F* integral of the mean response of each cell during each arousal state, normalized to low arousal (1–20% pupil max). Reliability was measured as the mean pairwise trial-by-trial Pearson's correlation coefficient of responses during each arousal state. Lifetime sparseness was $\left(1 - \left\{\left[\sum_{j=1,N} rj/N\right]^2 / \left[\sum_{j=1,N} r_j^2/N\right]\right\}\right) \Big/ (1 - 1/N)$, where $r_j$ was the response peak amplitude of the cell to tone *j*, and *N* was the total number of tones.

Total correlations (sum of signal and noise correlations) were quantified using a trial-by-trial response vector (*dF/F* integral during the tone**)** for each arousal level for each cell (31). To calculate $r_{signal}$, the temporal order of each cell's responses to repeated presentations of each tone were shuffled, abolishing noise correlations while maintaining trial-by-trial stimulus identity. Total and signal correlations were obtained by calculating Pearson's correlation coefficients for the unshuffled and shuffled response vectors, respectively, of cell pairs from the same experiment. A noise correlation value for each cell pair from each experiment was obtained by subtracting their signal correlation value from their total correlation value. To determine if arousal modulates $r_{noise}$ in a $r_{signal}$-related manner, mean noise correlations were calculated separately for cell pairs with signal correlations that increased (slope > 0) or decreased (slope < 0) with arousal.

For the nonlinear classifier, a population response matrix was created from the trial-by-trial responses for all cells of each experiment. The response matrices for a subset of randomly selected trials (75% of total) were used to train a K-nearest neighbors' classifier ($k = 10$ trials; standardized Euclidean distance metric) before testing the performance of the classifier on the remaining 25% of trials (100 iterations).

***Whole-cell recording.*** Recordings were made using the blind technique (32). Current-clamp recordings used pipettes filled with internal solution containing (in millimoles) 130 Kgluconate, 5 NaCl, 10 Hepes, 12 Na-phosphocreatine, 0.2 EGTA, 3 Mg-ATP, and 0.2 Na-GTP (pH 7.2, 305 mOsm). Voltage-clamp recordings used pipettes filled with (in millimoles) 130 Csgluconate, 10 Hepes, 5 TEA-Cl, 12 Na-phosphocreatine, 0.2 EGTA, 3 Mg-ATP, and 0.2 Na-GTP (pH 7.2, 310 mOsm). Series resistance ($R_s$ < 50 MOhms) was continuously monitored for stability. Recording depth (226 ± 11.3 μm from pia, $n = 31$) was determined from the micromanipulator *z* axis readout (MP-285, Sutter Instrument). Recordings were made with a Multiclamp 700A (Molecular Devices), digitized at 5–20 kHz, and acquired using AxoGraph. Potentials were not corrected for the liquid junction potential (~15 mV).

Responses were sorted by pupil diameter during the tone (1–35%, 36–65%, and 66–100%), averaged (≥5 trials) for each frequency, and baselined to tone onset. Cells were rejected if no ON response was >30 pA or >2 mV (voltage and current clamps, respectively). For current-clamp recordings, integral and peak amplitudes were measured 10–200 ms posttone onset. EPSP duration was measured at 25% of the peak. BF was the frequency with fastest EPSP onset (slope). In voltage-clamp recordings, ON response was measured as charge in a window of 20–30 ms posttone onset. NS was calculated as charge below baseline 75–125 ms posttone onset. Excitatory $I_m$ was measured relative to the most positive current value during each recording. Excitatory (inhibitory) charge above the baseline was calculated as the charge 10–100 ms posttone onset which was below (above) the baseline holding current. EPSC BF was determined from the peak amplitude of the response within 50 ms of tone onset. Cell responsiveness was determined with a Wilcoxon signed-rank test ($\alpha = 0.01$).

**Data Availability.** All data discussed in the paper will be made available to readers upon request.

**ACKNOWLEDGMENTS.** We are grateful to Chris Song and Elena Westeinde for technical support. We thank L. L. Looger, J. Akerboom, D. S. Kim, and the GENIE Project at Janelia Farm Research Campus for making GCaMP available. This work was supported by NIH Grants R01DC04682 and R01DC015239 to J.S.I. and NSF fellowships to S.K.A. and P.-A.L.

1. M. J. McGinley *et al*., Waking state: Rapid variations modulate neural and behavioral responses. *Neuron* **87**, 1143–1161 (2015).
2. K. D. Harris, A. Thiele, Cortical state and attention. *Nat. Rev. Neurosci.* **12**, 509–523 (2011).
3. E. Zagha, D. A. McCormick, Neural control of brain state. *Curr. Opin. Neurobiol.* **29**, 178–186 (2014).
4. S.-H. Lee, Y. Dan, Neuromodulation of brain states. *Neuron* **76**, 209–222 (2012).
5. M. Vinck, R. Batista-Brito, U. Knoblich, J. A. Cardin, Arousal and locomotion make distinct contributions to cortical activity patterns and visual encoding. *Neuron* **86**, 740–754 (2015).
6. A. Ayaz, A. B. Saleem, M. L. Schölvinck, M. Carandini, Locomotion controls spatial integration in mouse visual cortex. *Curr. Biol.* **23**, 890–894 (2013).
7. C. Bennett, S. Arroyo, S. Hestrin, Subthreshold mechanisms underlying state-dependent modulation of visual responses. *Neuron* **80**, 350–357 (2013).
8. C. M. Niell, M. P. Stryker, Modulation of visual responses by behavioral state in mouse visual cortex. *Neuron* **65**, 472–479 (2010).
9. Y. Fu *et al*., A cortical circuit for gain control by behavioral state. *Cell* **156**, 1139–1152 (2014).
10. P.-O. Polack, J. Friedman, P. Golshani, Cellular mechanisms of brain state-dependent gain modulation in visual cortex. *Nat. Neurosci.* **16**, 1331–1339 (2013).
11. J. Reimer *et al*., Pupil fluctuations track fast switching of cortical states during quiet wakefulness. *Neuron* **84**, 355–362 (2014).
12. P. J. Mineault, E. Tring, J. T. Trachtenberg, D. L. Ringach, Enhanced spatial resolution during locomotion and heightened attention in mouse primary visual cortex. *J. Neurosci.* **36**, 6382–6392 (2016).
13. D. M. Schneider, A. Nelson, R. Mooney, A synaptic and circuit basis for corollary discharge in the auditory cortex. *Nature* **513**, 189–194 (2014).
14. M. J. J. McGinley, S. V. V. David, D. A. A. McCormick, Cortical membrane potential signature of optimal states for sensory signal detection. *Neuron* **87**, 179–192 (2015).
15. M. Zhou *et al*., Scaling down of balanced excitation and inhibition by active behavioral states in auditory cortex. *Nat. Neurosci.* **17**, 841–850 (2014).
16. A. B. Saleem, A. Ayaz, K. J. Jeffery, K. D. Harris, M. Carandini, Integration of visual motion and locomotion in mouse visual cortex. *Nat. Neurosci.* **16**, 1864–1869 (2013).
17. L. Madisen *et al*., Transgenic mice for intersectional targeting of neural sensors and effectors with high specificity and performance. *Neuron* **85**, 942–958 (2015).
18. B. Willmore, D. J. Tolhurst, Characterizing the sparseness of neural codes. *Network* **12**, 255–270 (2001).
19. M. R. Cohen, A. Kohn, Measuring and interpreting neuronal correlations. *Nat. Neurosci.* **14**, 811–819 (2011).
20. B. B. Averbeck, P. E. Latham, A. Pouget, Neural correlations, population coding and computation. *Nat. Rev. Neurosci.* **7**, 358–366 (2006).
21. G. Rothschild, I. Nelken, A. Mizrahi, Functional organization and population dynamics in the mouse primary auditory cortex. *Nat. Neurosci.* **13**, 353–360 (2010).
22. D. E. Winkowski, P. O. Kanold, Laminar transformation of frequency organization in auditory cortex. *J. Neurosci.* **33**, 1498–1508 (2013).
23. E. B. Issa, X. Wang, Increased neural correlations in primate auditory cortex during slow-wave sleep. *J. Neurophysiol.* **109**, 2732–2738 (2013).
24. J. D. Downer, M. Niwa, M. L. Sutter, Task engagement selectively modulates neural correlations in primary auditory cortex. *J. Neurosci.* **35**, 7565–7574 (2015).
25. Y. Gu *et al*., Perceptual learning reduces interneuronal correlations in macaque visual cortex. *Neuron* **71**, 750–761 (2011).
26. J. M. Jeanne, T. O. Sharpee, T. Q. Gentner, Associative learning enhances population coding by inverting interneuronal correlation patterns. *Neuron* **78**, 352–363 (2013).
27. H. K. Kato, S. K. Asinof, J. S. Isaacson, Network-level control of frequency tuning in auditory cortex. *Neuron* **95**, 412–423.e4 (2017).
28. S. Arroyo, C. Bennett, S. Hestrin, Correlation of synaptic inputs in the visual cortex of awake, behaving mice. *Neuron* **99**, 1289–1301.e2 (2018).
29. H. Adesnik, Synaptic mechanisms of feature coding in the visual cortex of awake mice. *Neuron* **95**, 1147–1159.e4 (2017).
30. H. K. Kato, S. N. Gillet, J. S. Isaacson, Flexible sensory representations in auditory cortex driven by behavioral relevance. *Neuron* **88**, 1027–1039 (2015).
31. M. Pachitariu, D. R. Lyamzin, M. Sahani, N. A. Lesica, State-dependent population coding in primary auditory cortex. *J. Neurosci.* **35**, 2058–2073 (2015).
32. T. W. Margrie, M. Brecht, B. Sakmann, In vivo, low-resistance, whole-cell recordings from neurons in the anaesthetized and awake mammalian brain. *Pflugers Arch.* **444**, 491–498 (2002).